Electronic transport in nanostructures consisting of magnetic barriers

J. Q. You
Institute of Solid State Physics, Chinese Academy of Sciences, P.O. Box 1129, Hefei 230031, China
and Department of Physics, Xiangtan University, Xiangtan 411105, Hunan, China[*]

Lide Zhang
Institute of Solid State Physics, Chinese Academy of Sciences, P.O. Box 1129, Hefei 230031, China

P. K. Ghosh
Department of Physics, Xiangtan University, Xiangtan 411105, Hunan, China
and Department of Physics, Visva-Bharati University, Santiniketan 731235, West Bengal, India[†]

We study the transport properties of the nanostructures consisting of magnetic barriers produced by the deposition of ferromagnetic stripes on heterostructures. It is shown that the electron tunneling through multiple-barrier magnetic structures exhibits complicated resonant features. Due to the averaging of the transmission over half the Fermi surface, the conductance has, however, much simpler resonant structure. As for the single-barrier magnetic structures, our calculations show that the conductance preserves the main feature of the electron tunneling.

There have been numerous studies, both experimental and theoretical, devoted to the transport properties of semiconductor heterostructures. Present microfabrication technology[1] has made it possible to study the electronic transport in nanostructures, and considerable progress has been made in the understanding of a variety of transport phenomena.[2] Recently, much attention has been paid to electronic transport in inhomogeneous magnetic fields on the nanometer scale. Experimentally, fields of this kind can be realized with, for instance, the creation of magnetic dots,[3] the patterning of ferromagnetic materials,[4] and the deposition of superconducting materials on heterostructures.[5] In the theoretical aspect, the creation of superlattices by an inhomogeneous magnetic field[6] and the quantum transport of a two-dimensional electron gas (2DEG) in a weakly modulated magnetic field[7] have been investigated. Very recently, Matulis, Peeters, and Vasilopoulos[8] proposed four realistic magnetic barriers as produced by the deposition, on top of a heterostructure, of ferromagnetic and conducting stripes and superconducting plates interrupted by a stripe. They found that electron tunneling through square magnetic barriers is an inherently two-dimensional (2D) process, and that the magnetic barriers possess wave-vector filtering properties. However, the square magnetic barriers used in their study are not the proposed ones. In order to reveal the transport properties of realistic structures, in this paper we study the proposed magnetic barriers instead of the square ones.

As a prototype, two types of magnetic barriers are employed here, which are produced by the deposition, on top of a heterostructure, of a ferromagnetic stripe with magnetization (a) perpendicular and (b) parallel to the 2DEG located at a distance z_0 below the stripe; cf. Figs. 1(a) and 1(b) in Ref. 8. For these two structures, the magnetic barriers experienced by the 2DEG are given by[8]

$$\mathbf{B} = B(x,z_0)\hat{z} \; ,$$

$$B(x,z_0) = B_0[K(x+d/2,z_0) - K(x-d/2,z_0)] \; , \quad (1)$$

where (a) $B_0 = M_0 h/d$, $K(x,z_0) = 2xd/(x^2+z_0^2)$, and (b) $B_0 = M_0 h/d$, $K(x,z_0) = -z_0 d/(x^2+z_0^2)$, in which M_0 is the magnetization of the ferromagnetic stripe, and d and h are the thickness and height of the stripe, respectively. Here it has been assumed that $h/d \ll 1$ and $h/z_0 \ll 1$, which correspond to the extremely thin film. The magnetic barriers are shown in Figs. 1(a) and 1(b) for two different depths: $z_0 = 0.1$ (solid curve) and 0.3 (dashed curve). Also, the square magnetic barrier is presented in Fig. 1(c) for comparison.

The Schrödinger equation for the 2D system is

$$\frac{1}{2m^*}\{\mathbf{p} + e\,\mathbf{A}(x,z_0)\}^2 \Psi(x,y) = E\Psi(x,y) \; , \quad (2)$$

where m^* is the effective mass of the electron, and the Landau gauge $\mathbf{A}(x,z_0)$ is given by $\mathbf{A}(x,z_0) = (0, A(x,z_0), 0)$, in which

$$A(x,z_0) = B_0 d \ln\frac{(x+d/2)^2 + z_0^2}{(x-d/2)^2 + z_0^2} \; , \quad (3)$$

and

$$A(x,z_0) = B_0 d \left[\tan^{-1}\left(\frac{x-d/2}{z_0}\right) - \tan^{-1}\left(\frac{x+d/2}{z_0}\right)\right] \quad (4)$$

for cases (a) and (b), respectively. Assuming that $\Psi(x,y) = e^{iqy}\psi(x)$, where q is the wave vector of the electron in the y direction, one obtains that the wave function $\psi(x)$ obeys the following 1D Schrödinger equation:
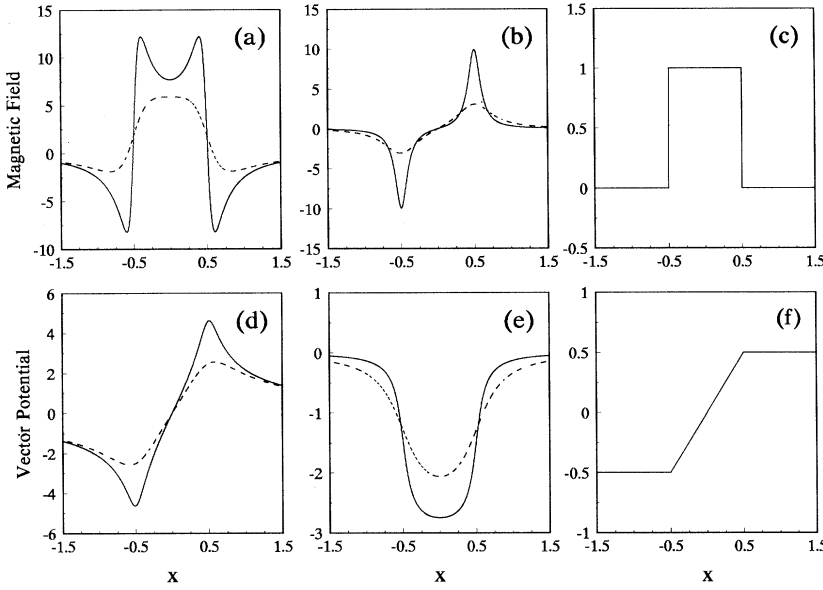
FIG. 1. Magnetic barriers and their corresponding vector potentials. For (a), (b), (d), and (e) the structural parameters are chosen to be $d=1$, and $z_0=0.1$ (solid curve) and 0.3 (dashed curve). In (c) and (f) a square magnetic barrier and its vector potential are shown for comparison. The spatial coordinate and length are in units of the magnetic length $l_B=\sqrt{\hbar/eB_0}$ in this figure and the following ones, the magnetic field is in units of B_0, and the vector potential in units of $B_0 l_B$.

$$\left\{ \frac{d^2}{dx^2} - [A(x,z_0)+q]^2 + 2E \right\} \psi(x) = 0 \ . \qquad (5)$$

Here we express the quantities in dimensionless units; the coordinate r is in units of the magnetic length $l_B=\sqrt{\hbar/eB_0}$, the vector potential $A(x,z_0)$ in units of $B_0 l_B$, and the energy E in units of $\hbar\omega_c=\hbar eB_0/m^*$. In Figs. 1(d)–1(f) we present the corresponding vector potentials for the magnetic barriers shown in Figs. 1(a)–1(c), respectively. It can be seen that the vector potential of the square magnetic barrier is drastically different from those of the barriers realized by the deposition of ferromagnetic stripes on heterostructures.

When the magnetic barrier is a square one, Eq. (5) is the Weber equation,[9] and within the barrier its solutions can be written as a linear combination of the Weber function $D_p(x)$ and its derivative.[8] However, no exact scheme is available for solving Eq. (5) with a more complicated vector potential. Thus we resort to an approximate method. For an arbitrary vector potential within the region $[x_-,x_+]$, we divide the region into $N(\gg 1)$ segments, of which each has width $D/N=(x_+-x_-)/N$,

and treat the vector potential as a constant $A(x_-+jD/N,z_0)$ in the jth segment $[x_-+jD/N,x_-+(j+1)D/N]$. Within this segment the Schrödinger equation (5) then becomes

$$\left\{ \frac{d^2}{dx^2} - [A(x_-+jD/N,z_0)+q]^2 + 2E \right\} \psi(x) = 0 \ , \qquad (6)$$

which has the plane-wave solution

$$\psi_j(x) = c_j e^{ik_j[x-(x_-+jD/N)]} + d_j e^{-ik_j[x-(x_-+jD/N)]} \ ,$$
$$x \in (x_-+jD/N, x_-+(j+1)D/N) \ , \qquad (7)$$

where k_j is given by $k_j = \{2E - [A(x_-+jD/N,z_0)+q]^2\}^{1/2}$.

From the wave-function-matching conditions at the boundaries of the segments, one obtains a set of coupled equations linking the amplitudes $\{c_j,d_j\}$,

$$\begin{bmatrix} c_{j+1} \\ d_{j+1} \end{bmatrix} = M(j+1,j) \begin{bmatrix} c_j \\ d_j \end{bmatrix}, \quad j=0,1,2,\ldots,N-1 \ , \qquad (8)$$

where

$$M(j+1,j) = \begin{bmatrix} \frac{1}{2}\left[1+\frac{k_j}{k_{j+1}}\right]e^{ik_jD/N} & \frac{1}{2}\left[1-\frac{k_j}{k_{j+1}}\right]e^{-ik_jD/N} \\ \frac{1}{2}\left[1-\frac{k_j}{k_{j+1}}\right]e^{ik_jD/N} & \frac{1}{2}\left[1+\frac{k_j}{k_{j+1}}\right]e^{-ik_jD/N} \end{bmatrix} . \qquad (9)$$

By successive multiplication of the transfer matrices given in Eq. (9), we are able to obtain the transfer matrix $M=(m_{ij})$ linking the amplitudes of the wave functions at the left and right ends, x_- and x_+, of the structure. As-

suming that the wave function on the left side of the structure is $\psi_-(x)=e^{ik_-(x-x_-)}+re^{-ik_-(x-x_-)}$, $x<x_-$, and the transmitted wave function on the right side $\psi_+(x)=te^{ik_+(x-x_+)}$, $x>x_+$, one can derive the

reflection and transmission coefficients

$$R = |r|^2 = |m_{21}/m_{22}|^2 ,$$

$$T = |t|^2 = 1 - |m_{21}/m_{22}|^2 .$$

(10)

For given energies and spatial regions within $[x_-, x_+]$, the wave vectors in Eq. (7) can be either real or imaginary. In our numerical calculations, we express the wave vectors k_j and k_{j+1} in Eq. (9) as double-precision complex quantities, and employ the double-precision complex exponential function for $\exp(ik_j D/N)$. Then multiplying the transfer matrices (9) can be realized in a unified way and performed accurately. Furthermore, it needs to be noted that, since the wave vector k_- of $\psi_-(x)$ should be real, energies obeying $E \geq \frac{1}{2}[A(x_-,z_0)+q]^2$ are allowed for transmission. With the transmission coefficient obtained, one can calculate the conductance[8]

$$G = G_0 \int_{-\pi/2}^{\pi/2} T(E_F, \sqrt{2E_F} \sin\phi) \cos\phi \, d\phi ,$$

(11)

where ϕ is the angle of incidence relative to the x direction; E_F is the Fermi energy; $G_0 = e^2 m v_F l/\hbar^2$, with l the length of the structure in the y direction; and v_F is the Fermi velocity. The conductance (11) is valid in the ballistic regime, which is derived as the electron flow averaged over half the Fermi surface.[10]

To demonstrate the reliability of the approximation method described above, we study the electron transmission through a structure consisting of the square magnetic barriers (see the inset of Fig. 2). Our results shown in Fig. 2 are calculated for three different values of the y component of the wave vector, $q = 0$ and ± 0.7, and the structural parameters are chosen to be $d = 1$ and $L = 3$. Comparing Fig. 2 with Fig. 4(a) in Ref. 8, one sees that our calculated results agree very well with those derived by Matulis, Peeters, and Vasilopoulos using the transfer-
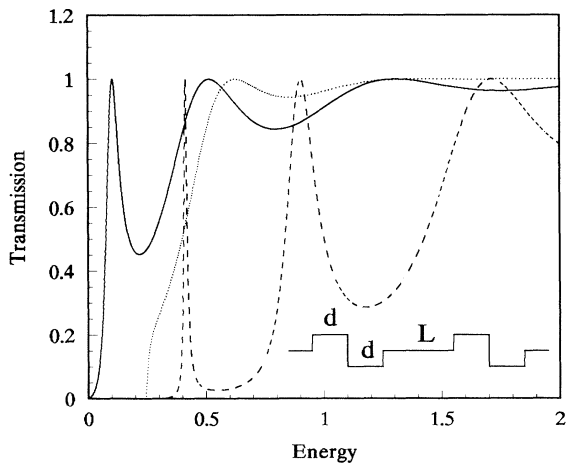

FIG. 2. Transmission coefficient for three different values of the y component of the wave vector, $q = 0$ (solid curve), 0.7 (dashed curve), and -0.7 (dotted curve). The magnetic structure is shown in the inset and its parameters are chosen to be $d = 1$ and $L = 3$. In this figure and the following ones, the energy is in units of $\hbar\omega_c = \hbar eB_0/m^*$.
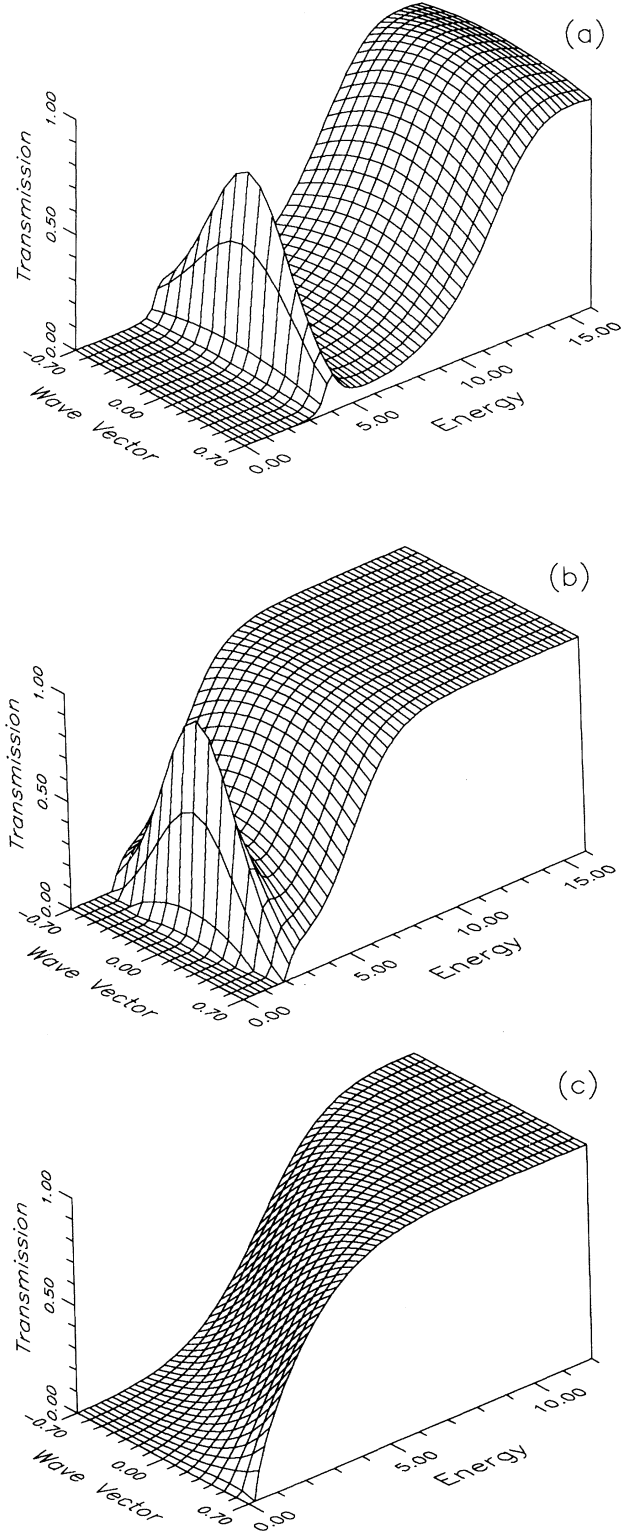

FIG. 3. Transmission coefficient for magnetic barriers presented in Figs. 1(a) and 1(b), where the structural parameters are chosen to be (a) $d = 1$ and $z_0 = 0.1$, (b) $d = 1$ and $z_0 = 0.3$ for the barrier shown in Fig. 1(a), and (c) $d = 1$ and $z_0 = 0.1$ for the barrier given in Fig. 1(b). The left and right ends of the barriers are located at $x_- = -1.5$ and $x_+ = 1.5$, respectively.

matrix approach in the framework of the Weber function formalism.

Figure 3 shows the electron transmission through the magnetic barriers presented in Figs. 1(a) and 1(b), as a function of the energy E and the wave vector q, where the structural parameters d and z_0 are chosen to be (a) $d = 1$ and $z_0 = 0.1$ and (b) $d = 1$ and $z_0 = 0.3$ for the magnetic barrier shown in Fig. 1(a), and (c) $d = 1$ and $z_0 = 0.1$ for the barrier given in Fig. 1(b). In our calculations the left and right ends of the barriers are assigned as $x_- = -1.5$ and $x_+ = 1.5$, respectively. The dependence of the electron transmission on both E and q is clearly seen. For the magnetic barrier shown in Fig. 1(a), the corresponding vector potential $A(x, z_0)$ is antisymmetric with respect to x. Our calculations show that the electron transmission is symmetric about the $q = 0$ plane; cf. Figs. 3(a) and 3(b). When $|q|$ is small, the term $[A(x, z_0) + q]^2$ in Eq. (5) is equivalent to a double-barrier electric potential, so a reso-

nant peak is expected in the low-energy region. Furthermore, it can also be seen from Figs. 3(a) and 3(b) that, when the parameter z_0 increases, both the resonant peak and the transmission step in the higher-energy region shift toward zero energy and squeeze each other. As for the magnetic barrier given in Fig. 1(b), the corresponding vector potential $A(x, z_0)$ is a symmetric function with respect to x and the transmission is not symmetric about the $q = 0$ plane. In Fig. 3(c) the asymmetry of the transmission is clearly demonstrated.

In Fig. 4 we present electron transmission through a structure consisting of two identical magnetic barriers, i.e., a barrier shown in Fig. 1(b) is followed by an identical one. The parameters are here chosen to be the same as in Fig. 3(c) but (a) $z_0 = 0.1$ and (b) $z_0 = 0.3$. The transmission exhibits complicated resonant structures, and its asymmetry about the $q = 0$ plane is clearly shown. Also, it can be seen that there are sharper resonant peaks in the low-energy region, and, with the parameter z_0 increasing, both the resonant peaks and the transmission step go toward zero energy and are pressed together. This feature is analogous to that observed in Figs. 3(a) and 3(b).

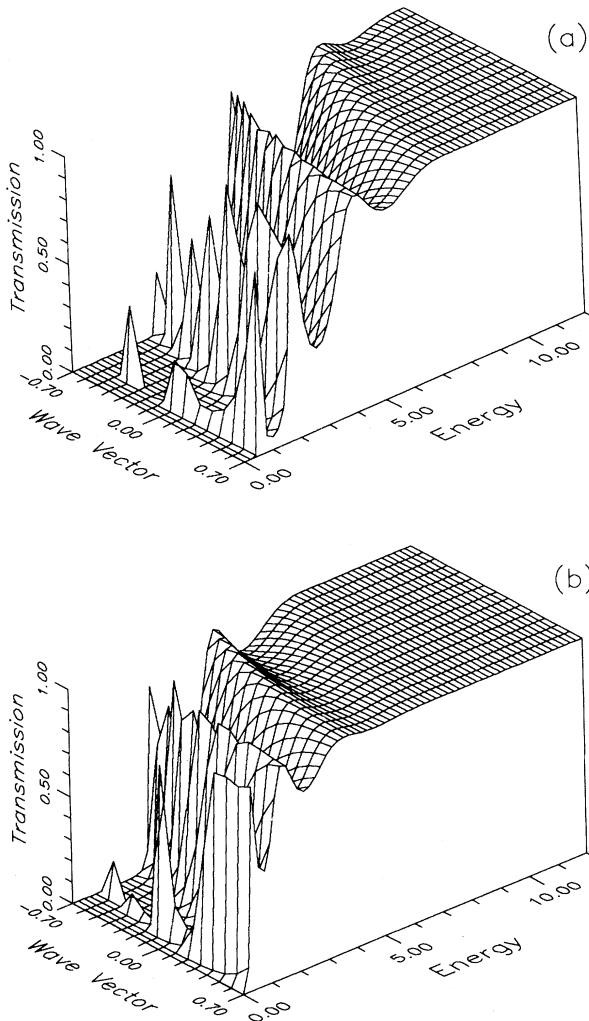Finally, we study the conductance through magnetic

FIG. 4. Transmission coefficient for a structure consisting of two magnetic barriers, in which a barrier shown in Fig. 1(b) is followed by an identical one. The parameters are the same as in Fig. 3(c), but (a) $z_0 = 0.1$ and (b) $z_0 = 0.3$.
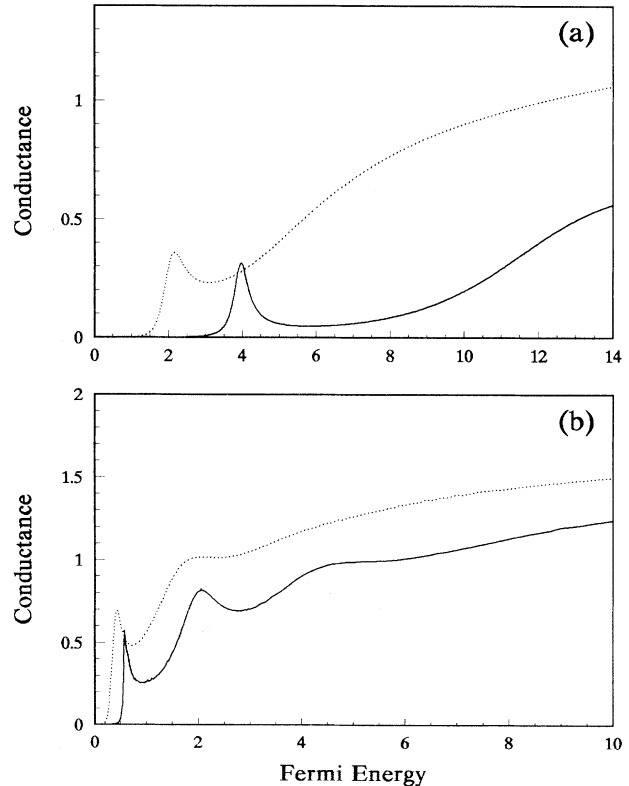

FIG. 5. Conductance through magnetic barriers. (a) A single-barrier structure, where the parameters are the same as in Figs. 3(a) and 3(b). (b) A double-barrier structure, where the structural configuration and its parameters are the same as in Fig. 4. Here the solid and dotted curves correspond to $z_0 = 0.1$ and 0.3, respectively, and the conductance is in units of $G_0 = e^2 m v_F l / \hbar^2$.

structures. Figure 5(a) shows the conductance through the magnetic barrier given in Fig. 1(a), where the parameters are chosen to be the same as in Figs. 3(a) and 3(b), and $z_0 = 0.1$ (solid curve) and 0.3 (dotted curve). Despite the averaging of $T(E,q)$ over half the Fermi surface, the main feature of the electron transmission is still reflected in the conductance. From Fig. 5(a) one sees that the conductance has a resonant peak in the low Fermi energy region. With z_0 increasing, the resonant peak and the step shift toward zero Fermi energy and are pressed together. In Fig. 5(b) we present the conductance through a structure consisting of two identical magnetic barriers. The structural configuration and its parameters are the same as those for Fig. 4. Here $z_0 = 0.1$ and 0.3 correspond to the solid and dotted curves, respectively. The conductance has a resonant structure, and its main feature is similar to that of Fig. 5(a). Though the transmission shows complicated resonant structures (see Fig. 4), the conductance does not, however, as a result of the averaging of the transmission over half the Fermi surface.

In summary, we have studied electronic transport in nanostructures consisting of magnetic barriers proposed by Matulis, Peeters, and Vasilopoulos. These barriers can be realized by the deposition of ferromagnetic stripes on heterostructures. Here two single-barrier magnetic structures are investigated, one of which shows a resonant peak in both the transmission and conductance. Also, we studied a double-barrier magnetic structure. It is shown that the conductance of this structure has two resonant peaks. Due to the averaging of the transmission over half the Fermi surface, the conductance does not preserve the complicated structures in the electron transmission. In this paper we studied, as examples, structures composed of one and two magnetic barriers. Extension to other structures consisting of more magnetic barriers is straightforward by means of the method used above. Because more barriers are involved, both the transmission and conductance then exhibit more and sharper resonant peaks.[11]

*Mailing address.

†Present address.

[1] See, e.g., M. L. Roukes *et al.*, in *Science and Engineering of 1- and 0-Dimensional Conductors*, edited by S. P. Beaumont and C. M. Sotomayor-Torres (Plenum, New York, 1989).

[2] See, e.g., S. Datta and M. J. McLennan, Rep. Prog. Phys. **53**, 1003 (1990), and references therein; M. Büttiker, in *Nanostructured Systems*, edited by M. Reed, Semiconductors and Semimetals Vol. 35 (Academic, San Diego, 1992), and references therein.

[3] M. A. McCord and D. D. Awschalom, Appl. Phys. Lett. **57**, 2153 (1990).

[4] M. L. Leadbeater *et al.*, J. Appl. Phys. **69**, 4689 (1991); K. M. Krishnan, Appl. Phys. Lett. **61**, 2365 (1992); R. Yagi and Y. Iye, J. Phys. Soc. Jpn. **62**, 1279 (1993).

[5] S. J. Bending, K. von Klitzing, and K. Ploog, Phys. Rev. Lett. **65**, 1060 (1990); A. K. Geim, Pis'ma Zh. Eksp. Teor. Fiz. **50**, 359 (1989) [JETP Lett. **50**, 389 (1990)].

[6] D. Yoshioka and Y. Iye, J. Phys. Soc. Jpn. **56**, 448 (1987); P. P. Vil'ms and M. V. Entin, Fiz. Tekh. Poluprovodn. **22**, 1905 (1988) [Sov. Phys. Semicond. **22**, 1209 (1988)].

[7] F. M. Peeters and P. Vasilopoulos, Phys. Rev. B **47**, 1466 (1993).

[8] A. Matulis, F. M. Peeters, and P. Vasilopoulos, Phys. Rev. Lett. **72**, 1518 (1994).

[9] Zhuxi Wang and Dunren Guo, *An Introduction to Special Functions* (Science, Beijing, 1965).

[10] M. Büttiker, Phys. Rev. Lett. **59**, 1761 (1986).

[11] J. Q. You and Lide Zhang (unpublished).